## Dark Matter Constraints from Isomeric <sup>178m</sup>Hf

D. S. M. Alves, S. R. Elliott, R. Massarczyk, S. J. Meijer, and H. Ramani <sup>1</sup>Los Alamos National Laboratory, Los Alamos, New Mexico 87545, USA <sup>2</sup>Stanford Institute for Theoretical Physics, Stanford University, Stanford, California 94305, USA

(Received 7 June 2023; revised 10 August 2023; accepted 11 September 2023; published 5 October 2023)

We describe a first measurement of the radiation from a  $^{178m}$ Hf sample to search for dark matter. The  $\gamma$ flux from this sample, possessed by Los Alamos National Laboratory nuclear chemistry, was measured with a Ge detector at a distance of 1.2 m due to its high activity. We search for y's that cannot arise from the radioactive decay of <sup>178m</sup>Hf but might arise from the production of a nuclear state due to the inelastic scattering with dark matter. The limits obtained on this  $\gamma$  flux are then translated into constraints on the parameter space of inelastic dark matter. Finally, we describe the potential reach of future studies with  $^{178m}$ Hf.

DOI: 10.1103/PhysRevLett.131.141801

There is irrefutable evidence for the existence of dark matter arising purely from gravitational interactions. Understanding its particle nature is one of the burning questions of 21st-century particle physics. Dark matter candidates at the weak scale arise naturally in theories beyond the standard model (SM), such as supersymmetry. Furthermore, weak scale massive particles with weak scale cross sections—the so-called "weakly interacting massive particles" (WIMPs)—are produced with the correct relic abundance when freezing out from thermal equilibrium in the early Universe (WIMP miracle). Direct, indirect, and collider searches for WIMPs have reported repeated null results, setting stringent limits on their model space. A review of the present status of the search for dark matter can be found in [1]. The derived limits are very restrictive, and the lack of an observation has motivated dark matter considerations beyond the classic WIMP description.

Among other alternative dark matter models are inelastic dark matter (iDM) [2–5] and strongly interacting dark matter (SIDM) [6–8]. While these models retain the salient features of thermal freeze-out, constraints on their parameter spaces are much less stringent, because the threshold energy required for a detectable dark matter-nucleus scattering event is often unavailable—in the case of iDM, due to the large inelastic splitting; and in the case of SIDM, due to the loss of dark matter kinetic energy from its interactions with the overburden rock above deep underground experiments. More specifically, in iDM models, dark matter-nucleus elastic scattering is suppressed, and the dominant scattering process requires an internal transition to an excited dark matter state. If the transition energy is greater than the available kinetic energy of the dark matter-nucleus system, this process is completely shut off, severely reducing the sensitivity to the iDM parameter space of present experiments focused on WIMPs. In the case of SIDM models, the large dark matter nuclear cross

section causes dark matter particles to thermalize through interactions with Earth, resulting in a velocity too low to produce a measurable interaction by the time they reach the detector's location deep underground. In particular, large scattering cross sections (much higher than electroweak strength) are still viable for significant swaths of parameter space of both SIDM and iDM models. While this is difficult to obtain with perturbative models of new physics at the TeV scale, composite dark matter models from a strongly interacting dark sector can naturally accommodate these properties [9–13].

In this Letter, we consider a recent proposal to use nuclear metastable states as exothermic-reaction targets for dark matter searches [14]. The isomer <sup>178m</sup>Hf has a large reservoir of available energy for transference to a dark matter particle, making it an intriguing candidate. Unfortunately, due to the relatively short half-life (31 yr) of this manmade isotope, a large number of target atoms also means significant radioactivity. In this Letter, we describe a first study of the  $\gamma$  spectrum of  $^{178m}$ Hf to derive first limits on dark matter interactions with this isotope.

The <sup>178m</sup>Hf sample used in this study was fabricated by the Los Alamos National Laboratory (LANL) nuclear chemistry division to produce <sup>172</sup>Hf for a <sup>172</sup>Hf/<sup>172</sup>Lu medical generator [15]. Later, this material was used to study the possibility of energy storage in nuclear isomers, specifically <sup>178m</sup>Hf. Reports of triggered isomer decay in <sup>178m</sup>Hf led to a further study [16], finding no evidence for the effect. The hafnium sample used for that experiment, and for this measurement, was extracted from a Ta target at the Los Alamos Meson Physics Facility accelerator at LANL [17]. The sample studied here is the second set as described in [16]. It is now relatively old, and Hf isotopes other than 178 m have decayed away, leaving a rather pure sample as indicated by the observed  $\gamma$  rays listed in Table I.

TABLE I. The stronger lines observed in the spectrum.

$E_{\gamma}$ [keV]	Origin	$E_{\gamma}$ [keV]	Origin	
55.3	<sup>178m</sup> Hf x rays	725.9	<sup>212</sup> Bi	
62.7	<sup>178</sup> mHf x ray	768.4	<sup>214</sup> Bi	
68.6	Au x-ray det. mat.	794.9	<sup>228</sup> Ac	
77.9	Au x-ray det. mat.	860.6	<sup>208</sup> Tl	
88.6	$^{178m}\mathrm{Hf}$	910.5	<sup>228</sup> Ac	
93.2	$^{178m}\mathrm{Hf}$	968.2	<sup>228</sup> Ac	
213.4	$^{178m}\mathrm{Hf}$	1093.5	<sup>208</sup> Tl sum	
216.7	$^{178m}\mathrm{Hf}$	1120.6	<sup>214</sup> Bi	
237.4	$^{178m}\mathrm{Hf}$	1238.4	<sup>214</sup> Bi	
257.6	$^{178m}\mathrm{Hf}$	1242.0	<sup>174</sup> Lu <sup>a</sup>	
277.3	$^{178m}\mathrm{Hf}$	1377.7	<sup>214</sup> Bi	
296.8	$^{178m}\mathrm{Hf}$	1460.2	$^{40}\mathrm{K}$	
325.6	$^{178m}\mathrm{Hf}$	1729.6	<sup>214</sup> Bi	
426.4	$^{178m}$ Hf	1764.8	<sup>214</sup> Bi	
454.0	$^{178m}$ Hf	1847.4	<sup>214</sup> Bi	
495.0	$^{178m}\mathrm{Hf}$	2103.6	<sup>208</sup> Tl esc. peak	
511.0	Annihilation	2117.8	<sup>214</sup> Bi	
535.0	$^{178m}$ Hf	2204.1	<sup>214</sup> Bi	
574.2	$^{178m}\mathrm{Hf}$	2448.4	<sup>214</sup> Bi	
583.5	<sup>208</sup> Tl	2614.5	<sup>208</sup> Tl	
608.9	<sup>214</sup> Bi			

<sup>a</sup>The weak line at 1241.8 keV most likely originates from Lu-174. It is seen in both the Hf and room background spectra, so it is not associated with the sample. A strong Lu source stored in this radiological controlled area might be the source of this  $\gamma$ .

Because of the sample's high activity (20–25 mR/hr on contact), the detector was placed at a distance of 1.2 m (4 ft) in order to minimize dead time from pile-up rejection. The detector was an ORTEC<sup>®</sup> Detective-X Ge detector [18]. The spectrum, from 974.2 s live time (1204 s run time) shown in Fig. 1, indicates some natural room background

lines from the U/Th/K decay chains along with the known  $^{178m}$ Hf lines. A list of the identified lines are given in Table I. Note that, above 600 keV, the spectrum is dominated by the natural background. Below 600 keV, the spectrum is dominated by  $^{178m}$ Hf emission.

The 31-yr metastable state at 2446 keV has a large spin  $J^{\pi}=16^+$ . Table II lists a number of Hf states which are prevented from being populated by  $\gamma$  transitions originating from the  $16^+$  metastable state due to the large spin change,  $\Delta J$ . An interaction with a heavy and slow dark matter particle, on the other hand, could overcome the  $\Delta J$  hindrance and catalyze transitions from the  $16^+$  metastable state to those (otherwise unpopulated) lower spin states, which, in turn, could decay via  $\gamma$  emission. Figure 2 depicts the  $^{178m}$ Hf level diagram showing the radioactive decay pathways in contrast to the dark-matter-induced pathways for a couple of the key transitions.

When a dark matter particle scatters off the isomeric nuclear state, the metastable nuclear energy can be tapped to excite the dark matter to an elevated internal energy state. The primary advantage of <sup>178m</sup>Hf is its large metastable state energy, which allows us to probe, for the first time in a direct detection experiment, dark matter mass splittings as high as  $\delta M_{\gamma} \sim \mathcal{O}(\text{MeV})$ . In particular, dark-matter-induced transitions of the isomeric state to the lower-energy states would be sensitive to the largest dark matter mass splittings. Unfortunately, most of the low-lying <sup>178</sup>Hf states are also populated through the SM radioactive decay of <sup>178m</sup>Hf and, therefore, suffer from large backgrounds and reduced iDM detection sensitivity. Therefore, we focus on dark-matterinduced transitions to higher-energy states not populated by the SM decay pathways and emit  $\gamma$ 's above  $\sim$ 600 keV in regions with reduced backgrounds. In Table II, we list only the excited  $^{178}$ Hf states and associated decay  $\gamma$ 's determined to be the most sensitive given these constraints (we note

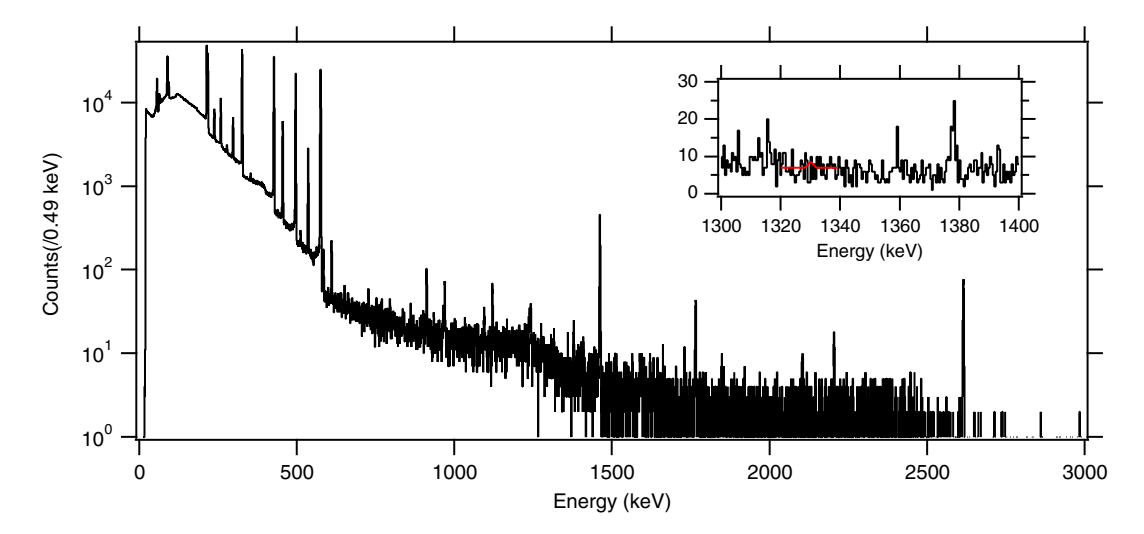


FIG. 1. The observed spectrum from the  $^{178m}$ Hf sample for a live time of 974.2 s. The inset shows the spectrum surrounding 1330 keV. A dark-matter-induced  $\gamma$  with this energy proved to be the most sensitive test. The superimposed curve shows a flat background with a Gaussian peak normalized to the 90% upper limit of 7.8 counts upon a region of interest background expectation of 44.2 counts.

TABLE II. The input parameters<sup>a</sup> and resulting 90% C.L. limits on the half-life  $T_{1/2}^{(j)}$  of the dark-matter-induced transition shown in Eq. (1). The smoking-gun signal for this process is the  $\gamma$  emitted in the decay of dark-matter-induced state <sup>178</sup>Hf $_j$  (fourth column). The relative detector efficiencies normalized to that for the 495-keV  $\gamma$ ,  $\epsilon_{\gamma}^{(j)}/\epsilon_{495}$ , were obtained from [18] and are assumed to carry uncorrelated uncertainties of  $\pm 20\%$ . The isomeric state of <sup>178</sup>mHf at 2446.1 keV has  $J^{\pi}=16^+$  and K=16.

Label j	State energy $E_j$ (keV)	State $J^{\pi}$ , $K$	$\gamma$ energy $E_{\gamma}^{(j)}$ (keV)	$\gamma$ branching ratio $b_{\gamma}^{(j)}$	Acceptance $\mathcal{A}_{\gamma}^{(j)}$	Rel. eff. $\epsilon_{\gamma}^{(j)}/\epsilon_{495}$	Background counts	Observed counts	$T_{1/2}^{(j)}$ (10 <sup>5</sup> yr)
1	1635.6	4+, 0	1542.2	$0.97 \pm 0.04$	0.83	0.41	$20.52 \pm 1.29$	17	> 1.56
2	1636.7	$5^{-}, 5$	1330.0	$0.57 \pm 0.03$	0.86	0.44	$44.23 \pm 1.98$	32	> 1.12
3	1640.5	$5^+, 4$	1333.8	$0.55 \pm 0.02$	0.86	0.44	$40.93 \pm 1.87$	40	> 0.52
4	1648.8	$6^{-}, 2$	1016.6	$0.60 \pm 0.04$	0.84	0.47	$75.97 \pm 2.52$	82	> 0.30
5	1651.5	$5^{-}, 1$	1344.9	$0.70 \pm 0.02$	0.86	0.44	$38.27 \pm 1.81$	41	> 0.51
6	1654.3	$4^{+}, 0$	1348.0	$0.68 \pm 0.21$	0.86	0.44	$36.99 \pm 1.81$	34	> 0.69
7	1691.1	$6^+, 2$	1059.0	$0.55 \pm 0.02$	0.83	0.47	$74.65 \pm 2.45$	50	> 1.21
8	1697.5	9-, 8	333.4	$1.00 \pm 0.00$	0.83	1.24	$6434.7 \pm 29.8$	6506	> 0.14
9	1747.1	$4^{-}, 2$	1440.6	$0.12 \pm 0.03$	0.84	0.44	$33.21 \pm 0.84$	31	> 0.13
10	1772.1	$0^{+}, 0$	1678.8	$1.00 \pm 0.11$	0.81	0.25	$15.55 \pm 0.81$	11	> 1.79
11	1788.6	$6^{+}, 4$	1156.3	$0.45 \pm 0.04$	0.81	0.47	$63.84 \pm 0.81$	67	> 0.26

<sup>&</sup>lt;sup>a</sup>The level energies, transition energies, and branching ratios are taken from the National Nuclear Data Center NuDat database [19] accessed March 2023.

that  $\gamma$ 's from the dark-matter-induced states at 1731.1 and 1781.3 keV are also ignored, because they fall in high background regions).

For the candidate  $\gamma$ 's listed in Table II, we obtain the number of observed and expected background counts

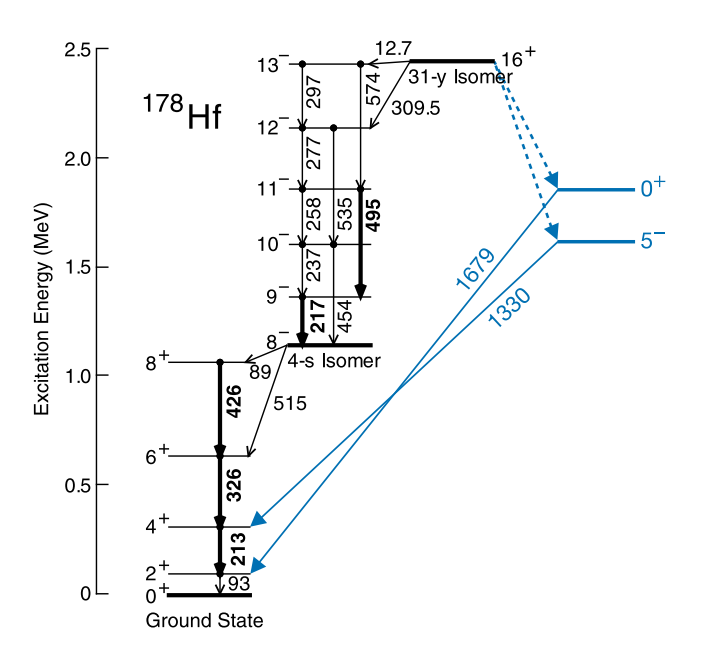


FIG. 2. The level diagram of  $^{178m}$ Hf. To the left (and in black) are the transitions that occur from the SM radioactive decay of the isotope. To the right (and in blue), we illustrate two dark-matter-induced transitions of significance: (i) the half-life of the  $16^+ \rightarrow 0^+$  transition (associated with the 1679 keV  $\gamma$ ) was the most strongly constrained by this work; (ii) the  $16^+ \rightarrow 5^-$  transition (associated with the 1330 keV  $\gamma$ ) provided the strongest constraint on the dark matter-nucleon cross section,  $\sigma_n$ , among the 11  $\gamma$ 's considered. This figure was adapted from Fig. 1 in [17].

within an optimized window centered on the  $\gamma$  energy. The expected background count (B) is obtained by performing a sideband fit of the data, assuming a linear background distribution. The width of the optimal window is deduced by maximizing  $\mathcal{A}_{\gamma}/\sqrt{B}$ , where  $\mathcal{A}_{\gamma}$  is the signal acceptance within the chosen window, assuming it follows a Gaussian distribution. For a continuum spectrum, the resulting signal acceptance within the optimal window is given by  $\mathcal{A}_{\gamma} \simeq 0.84$ ; however, since we collected a binned spectrum, the signal acceptance for each  $\gamma$  received a small correction to account for the bin edges. There were no observable peaks at any of the smoking-gun energies in Table II.

To establish our notation, consider the process in which a dark matter particle upscatters off the isomeric nuclear state  $^{178m}\!\mathrm{Hf}$ , causing the nucleus to transition to a lower-energy-level  $^{178}\!\mathrm{Hf}_{j}$ :

$$\chi + {}^{178m}\text{Hf} \to \chi^* + {}^{178}\text{Hf}_j.$$
 (1)

We will denote the inelastic cross section for this process by  $\sigma_{\rm inel}^{(j)}$ . The produced state  $^{178}{\rm Hf}_{j}$  can then deexcite via emission of a  $\gamma$  of energy  $E_{\gamma}^{(j)}$  with a branching ratio given by  $b_{\gamma}^{(j)}$ . The expected signal count for the process described above,  $S_{\gamma}^{(j)}$ , is given by

$$S_{\gamma}^{(j)} = N_T \Delta t \times (\sigma_{\text{inel}}^{(j)} \Phi_{\gamma}) \times (b_{\gamma}^{(j)} \mathcal{A}_{\gamma}^{(j)} e_{\gamma}^{(j)}), \tag{2}$$

where  $N_T$  is the number of target <sup>178m</sup>Hf nuclei;  $\Delta t = 974.2$  s is the live time;  $\Phi_{\chi}$  is the dark matter flux; and  $\mathcal{A}_{\gamma}^{(j)}$  and  $\varepsilon_{\gamma}^{(j)}$  are, respectively, the signal acceptance within the

region of interest and detection efficiency for the  $\gamma$  emitted in the decay of  $^{178}{\rm Hf}_{i}$ .

The number of target atoms  $N_T$  can be deduced from the SM activity of the Hf sample. In particular, the SM decay chain of  $^{178m}$ Hf produces a 495-keV  $\gamma$  line with a probability  $p_{495}=0.736\pm0.014$  [20]. The number of 495-keV  $\gamma$  counts observed during our live time,  $S_{495}=96\,808\pm395$ , relates to  $N_T$  via

$$N_T = \frac{\tau_{\text{isomer}}}{\Delta t} \frac{S_{495}}{p_{495}\epsilon_{495}},\tag{3}$$

where  $\tau_{\rm isomer}=1.41\times 10^9~{\rm s}$  is the lifetime of  $^{178m}{\rm Hf}$  and  $\varepsilon_{495}$  is the detection efficiency for the 495-keV  $\gamma$  line. The detector resolution at 495 keV is 1.15 keV FWHM. Also note that  $S_{495}$  was determined by a Gaussian fit to the peak, and, therefore, we have automatically set its acceptance to  $\mathcal{A}_{495}=1$  in Eq. (3).

Combining (2) and (3), we can express the dark matter event rate [i.e., number of scattering events in (1) per unit time per target nucleus] as

$$\sigma_{\text{inel}}^{(j)} \Phi_{\chi} = \tau_{\text{isomer}}^{-1} \frac{S_{\gamma}^{(j)}}{S_{495}} \frac{p_{495} \epsilon_{495}}{b_{\gamma}^{(j)} \mathcal{A}_{\gamma}^{(j)} \epsilon_{\gamma}^{(j)}}. \tag{4}$$

The corresponding half-life for this dark-matter-induced transition is simply related to (4) via

$$T_{1/2}^{(j)} = \frac{\log 2}{\sigma_{\text{inel}}^{(j)} \Phi_{\gamma}}.$$
 (5)

By performing a profiled log-likelihood fit [21] of the signal strength for each of the 11  $\gamma$  lines considered, we obtained 90% confidence level (C.L.) limits on the half-lives  $T_{1/2}^{(j)}$ , given in Table II.

The inelastic cross section for the process in (1),  $\sigma_{\text{inel}}^{(j)}$ , can be related to the model-dependent dark matter-nucleon cross section  $\sigma_n$  using the formalism of [14]. We used this relation to translate our limits into constraints on the parameter space of iDM, namely,  $\sigma_n$  versus the iDM mass splitting  $\delta M_{\chi}$  for a benchmark iDM mass of  $M_{\chi}=1$  TeV. Note that the transition with the most strongly constrained half-life does not necessarily provide the strongest constraint on  $\sigma_n$ . That is because the nuclear form factor, which suppresses the transition rate in (1), depends not only on the momentum transfer q and change in angular momentum  $\Delta J$ , but also on K-selection rules. Specifically, each nuclear state has a K-quantum number given by the projection of its angular momentum on its symmetry axis (see Table II), and transitions with  $\Delta K$  greater than the multipolarity of the emitted radiation suffer from an additional suppression, the so-called "K hindrance." Among the 11 transitions considered, j=2 provides the strongest constraint on  $\sigma_n$ , since it has the second smallest  $\Delta K (= 11)$ , and the observed

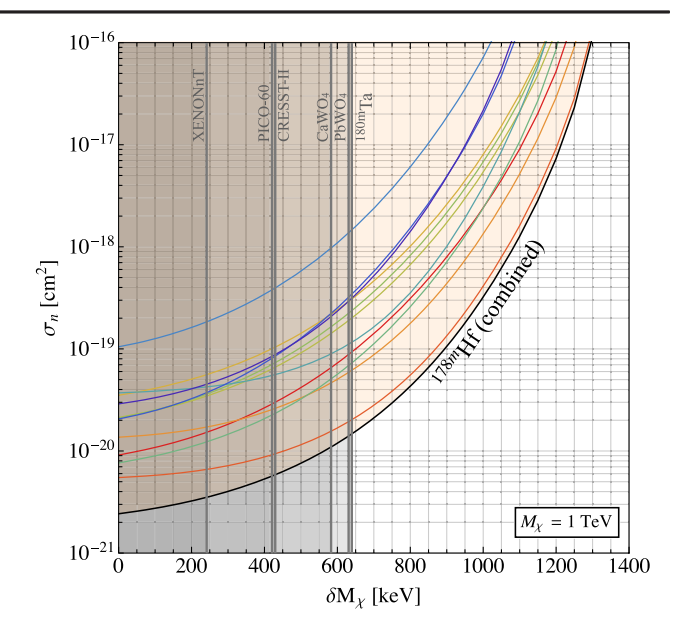


FIG. 3. The 90% C.L. exclusion limits on the parameter space of inelastic dark matter, assuming a standard halo model with local dark matter density  $\rho_{\chi}=0.3~{\rm GeV/cm^3}$  and galactic escape velocity  $v_{\rm esc}=600~{\rm km/s}$ . The black curve shows the combined limit from all 11  $\gamma$ 's, and the shaded gray regions show previous existing limits [22–28]. The 11 colored curves show the limits from each individual  $\gamma$  line in Table II. Following the j-label convention of Table II and fixing  $\delta M_{\chi}=700~{\rm keV}$ , the order of the 11 colored curves, from stronger to weaker exclusion, is j=2,3,7,1,8,5,6,4,11,10,9.

counts for its associated  $\gamma$  line of 1330 keV showed a  $\sim 2\sigma$  deficit relative to the background expectation. We can contrast the constraining power of j=2 with that of other transitions. For example, while j=8 has the smallest  $\Delta K(=8)$ , its associated 333.4-keV  $\gamma$  line lies in a region with substantial backgrounds ( $\sim$ 2 orders of magnitude larger than the backgrounds for the other lines), which significantly weakens its dark matter constraining power. As another example, transitions j=1 and j=10 have the most strongly constrained half-lives but also the largest  $\Delta K(=16)$ , which suppresses their rate for  $\delta M_{\chi} \gtrsim 600$  keV. For further technical details, we refer the reader to [14], where the relevant formulas and discussion of this relation can be found in Secs. IV and VI.

Finally, we performed a joint log-likelihood fit of the signal strength for all 11  $\gamma$ 's combined. Our results are shown in Fig. 3.

For  $\delta M_{\chi} \gtrsim 640$  keV, our experimental limit on  $\sigma_n$  is the best to date, albeit dark matter models with such large cross sections would necessarily come from composite dynamics and might face model-building challenges. The strongest competing constraint in the large mass splitting region  $\delta M_{\chi} \gtrsim 400$  keV comes from searches using the tantalum metastable state  $^{180m}$ Ta. Experiments with samples containing a large number of  $^{180m}$ Ta nuclei provide interesting limits on SIDM and iDM models [23,29–31]. Still, the

comparably lower metastable energy of  $^{180m}$ Ta (77.2 keV [32]) limits its sensitivity to  $\delta M_{\chi} \lesssim 600$  keV. Other existing experimental results are described in [22], with specific limits derived from data for PbWO<sub>4</sub> [24], CaWO<sub>4</sub> [25], CRESST-II [26], PICO-60 [27], and XENONnT [28].

A number of improvements and options for future measurements are possible. A longer run time and the use of a shielded detector could improve sensitivity by a factor of ~10. A high-efficiency Ge-detector array similar to Advanced Gamma Tracking Array [33]—with a large solid angle acceptance and detectors distant enough from the source so as to have a manageable rate—could further improve sensitivity by an additional factor of ~100.

The Hf measurements reported here were performed at a surface site and, therefore, were not sensitive to viable parameter space in SIDM. By deploying the Hf sample and a detector underground, one could probe the effects of a dark matter traffic jam [14] in models of SIDM (both elastic and inelastic).

Ideally, one would like a very large sample of the Hf isomer. The Ta target for this sample was used as a dedicated beam stop from which the Hf was extracted by radiochemistry [15]. If feasible, processing additional targets could produce a large quantity of <sup>178</sup>mHf; however, the cost of the required radiochemistry would have to be weighed against the science reach. Furthermore, practical difficulties associated with the high radioactivity of the sample would need to be overcome.

We thank Evelyn Bond and Athena Marie Marenco for assisting with access to the sample. We gratefully acknowledge support from the U.S. Department of Energy Office of Science and from the Los Alamos National Laboratory's Directed Research and Development (LDRD) Program for this work.

- \*elliotts@lanl.gov
- [1] A. Boveia, T. Y. Chen, C. Doglioni, A. Drlica-Wagner, S. Gori, W. H. Lippincott, M. E. Monzani, C. Prescod-Weinstein, B. Shakya, T. R. Slatyer, N. Toro, M. Williams, L. Winslow, P. Tanedo, Y.-T. Tsai, J. Yu, and T.-T. Yu, Snowmass 2021 Cross Frontier Report: Dark Matter Complementarity (Extended Version), arXiv: 2210.01770.
- [2] D. Smith and N. Weiner, Phys. Rev. D **64**, 043502 (2001).
- [3] B. Feldstein, P. W. Graham, and S. Rajendran, Phys. Rev. D 82, 075019 (2010).
- [4] M. Pospelov, N. Weiner, and I. Yavin, Phys. Rev. D 89, 055008 (2014).
- [5] J. Bramante, P. J. Fox, G. D. Kribs, and A. Martin, Phys. Rev. D 94, 115026 (2016).
- [6] D. Hooper and S. D. McDermott, Phys. Rev. D 97, 115006 (2018).
- [7] V. De Luca, A. Mitridate, M. Redi, J. Smirnov, and A. Strumia, Phys. Rev. D 97, 115024 (2018).

- [8] D. A. Neufeld, G. R. Farrar, and C. F. McKee, Astrophys. J. 866, 111 (2018).
- [9] S. Nussinov, Phys. Lett. 165B, 55 (1985).
- [10] J. Bagnasco, M. Dine, and S. D. Thomas, Phys. Lett. B 320, 99 (1994).
- [11] D. S. M. Alves, S. R. Behbahani, P. Schuster, and J. G. Wacker, Phys. Lett. B 692, 323 (2010).
- [12] M. Lisanti and J. G. Wacker, Phys. Rev. D 82, 055023 (2010).
- [13] D. Spier Moreira Alves, S. R. Behbahani, P. Schuster, and J. G. Wacker, J. High Energy Phys. 06 (2010) 113.
- [14] M. Pospelov, S. Rajendran, and H. Ramani, Phys. Rev. D 101, 055001 (2020).
- [15] W. Taylor, J. G. Garcia, V. T. Hamilton, R. C. Heaton, D. J. Jamriska, M. A. Ott, D. R. Phillips, and S. D. Radzinski, J. Radioanal. Nucl. Chem. 236, 155 (1998).
- [16] I. Ahmad, J. C. Banar, J. A. Becker, T. A. Bredeweg, J. R. Cooper, D. S. Gemmell, A. Kraemer, A. Mashayekhi, D. P. McNabb, G. G. Miller, E. F. Moore, P. Palmer, L. N. Pangault, R. S. Rundberg, J. P. Schiffer, S. D. Shastri, T. F. Wang, and J. B. Wilhelmy, Phys. Rev. C 71, 024311 (2005).
- [17] I. Ahmad, J. C. Banar, J. A. Becker, D. S. Gemmell, A. Kraemer, A. Mashayekhi, D. P. McNabb, G. G. Miller, E. F. Moore, L. N. Pangault, R. S. Rundberg, J. P. Schiffer, S. D. Shastri, T. F. Wang, and J. B. Wilhelmy, Phys. Rev. Lett. 87, 072503 (2001).
- [18] ORTEC, 801 South Illinois Ave., Oak Ridge, TN 37830, USA, https://www.ortec-online.com.
- [19] E. Achterberg, O. Capurro, and G. Marti, Nucl. Data Sheets **110**, 1473 (2009).
- [20] M. B. Smith, P. M. Walker, G. C. Ball, J. J. Carroll, P. E. Garrett, G. Hackman, R. Propri, F. Sarazin, and H. C. Scraggs, Phys. Rev. C 68, 031302(R) (2003).
- [21] G. Cowan, *Statistical Data Analysis* (Oxford University Press, Oxford, 1998).
- [22] N. Song, S. Nagorny, and A. C. Vincent, Phys. Rev. D 104, 103032 (2021).
- [23] B. Lehnert, H. Ramani, M. Hult, G. Lutter, M. Pospelov, S. Rajendran, and K. Zuber, Phys. Rev. Lett. 124, 181802 (2020)
- [24] J. W. Beeman et al., Eur. Phys. J. A 49, 50 (2013).
- [25] A. Münster *et al.*, J. Cosmol. Astropart. Phys. 05 (2014) 018.
- [26] G. Angloher et al., Eur. Phys. J. C 76, 25 (2016).
- [27] C. Amole *et al.* (PICO Collaboration), Phys. Rev. D **93**, 052014 (2016).
- [28] E. Aprile *et al.* (XENON Collaboration 7), Phys. Rev. Lett. 121, 111302 (2018).
- [29] B. Lehnert, M. Hult, G. Lutter, and K. Zuber, Phys. Rev. C 95, 044306 (2017).
- [30] R. Cerroni, S. Dell'Oro, A. Formicola, S. Ghislandi, L. Ioannucci, M. Laubenstein, B. Lehnert, S. S. Nagorny, S. Nisi, and L. Pagnanini, arXiv:2305.17238.
- [31] I. J. Arnquist et al., arXiv:2306.01965.
- [32] E. McCutchan, Nucl. Data Sheets 126, 151 (2015).
- [33] A. Bracco, G. Duchêne, Z. Podolyák, and P. Reiter, Prog. Part. Nucl. Phys. 121, 103887 (2021).